CRYSTAL GROWTH & DESIGN
2009
VOL. 9, NO. 6
2690–2699

Crystal-Growth Behavior in Ca−Mg Carbonate Bacterial Spherulites

Antonio Sánchez-Navas,*[,†,‡] Agustín Martín-Algarra,[‡,§] María A. Rivadeneyra,[||] Santiago Melchor,[⊥] and José Daniel Martín-Ramos[†]

Departamento de Mineralogía y Petrología, Facultad de Ciencias, Universidad de Granada, IACT-CSIC, Campus Universitario de Fuentenueva, Departamento de Estratigrafía y Paleontología, Facultad de Ciencias, Universidad de Granada, IACT-CSIC, Campus Universitario de Fuentenueva, Departamento de Microbiología, Facultad de Farmacia, Universidad de Granada, Campus Universitario de Cartuja, and Departamento de Química Orgánica, Facultad de Ciencias, Universidad de Granada, Campus Universitario de Fuentenueva, 18071-Granada, Spain

Received December 4, 2008; Revised Manuscript Received February 20, 2009

ABSTRACT: Spherulites composed of aragonite, magnesian calcite, and calcian-magnesian (-manganoan) kutnahorite-type carbonates were precipitated by two halophilic bacterial strains in porous solid as well as liquid media at high salinity. Although Mg and Ca are geochemically similar elements, Ca is preferentially incorporated into aragonite structures in liquid media whereas Mg remains in the solution and/or precipitates to form struvite crystals. In solid media, crystal growth features clearly correlate with reticular parameters and the Mg content of the Ca−Mg and Ca−Mg(Mn) carbonates. The increased salinity in these media leads to the incorporation of Mg (and Mn) into the carbonate structure under growth conditions farther and farther from equilibrium. Although calcite is the stable phase in the Earth surface environments, carbonates denser than pure calcite, like aragonite and Mg-rich calcite, are kinetically favored in the studied bacterial precipitates.

Introduction

Biomediated bacterial precipitation in nature and in laboratory experiments produce many different biominerals,[1] among them metal carbonates, with amazingly complex crystal morphologies (bioliths) changing from polyhedral forms to dumbbells and spherulites.[2,3] The occurrence of the latter in the fossil record has prompted some authors to consider such morphologies as biomarkers,[4] although they are commonly produced in biotic and abiotic experiments.[5−7]

Many bacterial precipitates can be called "mesocrystals" as they are superstructures formed by the aggregation of nanocrystal building units,[8] and are frequently closely associated with amorphous precursors.[9] These biominerals may help to understand nucleation and crystal growth of new organic−inorganic hybrid materials that are crystallized by oriented aggregation of primary nanoparticles nucleated on natural or artificial organic templates (bacterial surfaces, exopolymeric substances, or organic additives), instead of by classical ion-by-ion or single molecule attachment. Precipitation of calcium carbonate nanoparticles on bacterial cells may have been one of the dominant modes of carbonate formation throughout the geologic record.[10]

Carbonate spherulitic bioliths that are commonly precipitated by many different types of bacteria in natural sedimentary environments and in artificial culture media are frequently formed by calcium and magnesium carbonate minerals such as aragonite, magnesian calcite and dolomite, which are, however, thermodynamically metastable phases under Earth surface conditions.[11] Consequently, an understanding of the kinetically favored precipitation of Ca−Mg carbonate minerals, in particular those precipitated by bacteria, requires knowledge of the microenvironmental factors that favor their precipitation, together with an atomistic interpretation of the interaction between the culture media and the carbonate crystal at the growing interface.

Studies on the crystal−solution interface in Mg-bearing carbonates provide new perspectives for understanding the surface-structure controls on Mg incorporation during Ca−Mg carbonate crystal growth.[12] Folk suggested that Mg^{2+} concentration in magnesian calcite controls morphology of crystals precipitated from $Ca^{2+}-Mg^{2+}-CO_3^{2+}$ aqueous solutions with a composition close to that of seawater.[13] Given and Wilkinson indicated that morphology is controlled by the crystal growth rate rather than by the Mg:Ca ratio of the solution.[14] The presence of Mg seems to play an important role in the precipitation of low crystalline calcium carbonates and in particular for the formation of amorphous calcium carbonates.[9] Under certain growth conditions, Mg^{2+} and other divalent cations such as Ba^{2+}, Sr^{2+}, Co^{2+} and Mn^{2+} can be incorporated into the carbonate structure, this having major consequences for crystal morphology.[6] The distribution coefficient of trace elements between crystals and solutions depends on the growth rate.[15]

In a previous study, Rivadeneyra et al. precipitated several types of Ca and Ca−Mg carbonate spherulites, among them and for the first time in halophilic bacterial cultures, spherulites with peculiar dendritic surface textures formed by a Ca−Mg carbonate phase with X-ray features and unit-cell size corresponding to that of kutnahorite, a Ca−Mn(Mg, Fe) carbonate of the dolomite group, but without Mn, which was absent in the culture media.[16] In this study, we describe the compositional, structural, and textural features of similar spherulitic bioliths formed by Ca−Mg(Mn) carbonate minerals precipitated by two bacterial strains in different culture media at high salinity. Also, we explain the crystal-growth features of the diverse types of spherulites in relation to salinity and type of culture medium. Finally, we propose a relation between the mineral structure,

* To whom correspondence should be addressed. Department of Mineralogy and Petrology, Faculty of Sciences and IACT-CSIC, University of Granada, 18071-Granada, Spain. Tel: +34 958246614. Fax: +34 958243368. E-mail: asnavas@ugr.es.
† Departamento de Mineralogía y Petrología, Facultad de Ciencias.
‡ IACT-CSIC.
§ Departamento de Estratigrafía y Paleontología, Facultad de Ciencias.
|| Departamento de Microbiología, Facultad de Farmacia.
⊥ Departamento de Química Orgánica, Facultad de Ciencias.

10.1021/cg801320p CCC: $40.75
Published on Web 04/03/2009

Table 1. Mineralogy, Type of Culture, and Precipitation Conditions

mineralogy	culture	salts (%)	Mg (%)	Mg/Ca molar relation	$MnCl_2 \cdot 4H_2O$ (%)
aragonite	*Ch. marismortui*(liquid media)	2.5	0.09	1.5	0
magnesian calcite	*H. anticariensis*(solid media)	2.5	0.09	1.5	0
magnesian calcite	*Ch. marismortui* (solid media)	2.5	0.09	1.5	0
Ca−Mg kutnahorite-type	*H. anticariensis* (solid media)	7.5	0.27	4.1	0
Ca−Mg(Mn) kutnahorite-type	*Ch. marismortui* (solid media)	7.5	0.27	4.1	0.1

Table 2. Composition and Crystallographic Data

		unit-cell axes (Å)			
mineralogy (bacterium)	composition	*a*	*b*	*c*	crystalline mosaic size (nm)
aragonite (*Ch. marismortui*)	$CaCO_3$	4.948	7.985	5.746	49 ± 6
Mg calcite (*H.anticariensis*)	$Ca_{0.98}Mg_{0.02}CO_3$	4.956	4.956	16.978	35 ± 5
Mg calcite (*Ch. marismortui*)	$Ca_{0.85-0.95}Mg_{0.15-0.05}CO_3$	4.955	4.955	16.789	55 ± 12
Ca−Mg kutnahorite-type (*H. anticariensis*)	$Ca_{0.67-0.77}Mg_{0.33-0.23}CO_3$	4.875	4.875	16.334	14 ± 1
Ca−Mg(Mn) kutnahorite-type (*Ch. marismortui*)	$Ca_{0.65-0.75}Mg_{0.35-0.23}Mn_{0-0.02}CO_3$	4.879	4.879	16.375	13 ± 3

the crystal growth behavior for Ca−Mg(Mn) carbonate spherulites and the kinetics of the bacterial precipitation process.

Experimental Section

Precipitation Experiments. In a previous study, bioliths made of spherulites formed by several Ca−Mg carbonate minerals and of struvite crystals were precipitated in liquid and solid media at different salt concentrations by *Chromohalobacter marismortui*, a moderately halophilic bacterium.[16] The experiment in solid media has been repeated, but in this case (1) using this bacterium strain after slightly modifying the culture medium with a solution of $MnCl_2 \cdot 4H_2O$ and (2) using a new bacterial strain.

The microorganisms used in this study were *Halomonas anticariensis* strain FP35^T (=LMG 22089^T = CECT 5854^T) and *Chromohalobacter marismortui* ATCC 17056^T (=CCM 3518^T), both Gram-negative rod, motile by peritrichous flagella, non-spore-forming, chemo-organotrophic and strictly aerobic bacteria.[17] The culture media had the following composition (wt/vol): 1% yeast extract, 0.5% proteose-peptone, 0.1% glucose, and 0.4% calcium acetate. The media were supplemented with a balanced mixture of sea salts to final concentrations of 2.5% or 7.5% (wt/vol), and 0.1% $MnCl_2 \cdot 4H_2O$ was added to one *Ch. marismortui* culture (Table 1). The pH was adjusted to 7.2 with 1 M KOH. A solid transport media with low porosity was achieved by adding 20 g/L of "Bacto-Agar". Bacteria were surface inoculated onto solid media and incubated at 32 °C for 30 days. Controls consisted of noninoculated culture media. The plates were examined periodically by light microscopy for the presence of precipitates.

Observation shows that *H. anticariensis* and *Ch. marismortui* cultures in solid media precipitate spherulitic bioliths. In both cases, the mineralogy changed (Table 1) and the size and number of spherulites increased with time and salt content, whereas no precipitation occurred in the control. The precipitates formed were removed from the medium for textural, compositional and mineralogical analysis; from solid media by cutting out agar blocks and placing them in a boiling water bath until the agar dissolved. The supernatants were decanted and the sediments resuspended and washed in distilled water until the precipitates were free of impurities, to be finally air-dried at 37 °C.

Methods. The precipitates were analyzed by powder X-ray diffraction (PXRD). Data were processed using XPowder program.[18] Crystalline mosaic size was obtained from Willianson−Hall plot using integral breadth as a measure of pure diffraction broadening after instrumental factors correction and $K\alpha_2$ stripping.[19] The composition of the spherulites (Table 2) was determined using a LEO1430VP scanning electron microscope equipped with an EDX system, model INCA350, for microanalysis. Diverse Mg−Ca-bearing silicates and oxides were used as standards for quantification of Ca, Mg, and Mn. High-resolution secondary electron images of carbon-coated samples were produced with a field-emission scanning electron microscope (FESEM) LEO 1525. During sample preparation, carbon coating was carefully performed to avoid, or minimize, the formation of artifacts that could change the morphology of the original material at nanometer scale.

Results

Mineralogy and Composition. For the purposes of this study, diverse types of spherulites were selected, each formed by only one type of carbonate mineral, but under different conditions (Table 1): aragonite, two magnesian calcites, each precipitated by *H. anticariensis* and *C. marismortui*, and two Ca−Mg kutnahorite-type carbonates, with and without traces of Mn) and precipitated by *Ch. marismortui* and *H. anticariensis*, respectively. The carbonate bioliths studied were spherulitic precipitates quite similar to those previously obtained by Rivadeneyra et al.[16] The size of the spherulites changed from 1−2 μm to >1 mm, but they were frequently comprised between 10 μm and 0.2 mm, in all cultures. Independently of their mineralogical and chemical composition or of the culture media where they were precipitated (Table 1), the spherulites were invariably surrounded and sometimes bonded together by organic pellicles that partially disappeared during washing. These gels were, however, more frequently observed in spherulites precipitated in solid media.

The precipitates found in solid media formed a changing mineral sequence at progressively higher salt concentrations (Table 1). At 2.5% salts, the mineral composition was exclusively magnesian calcite (Table 2). At 7.5% salts, spherulites were composed of a mixture of magnesian calcite plus a rhombohedral calcian−magnesian carbonate phase with lattice parameters corresponding to that of mineral kutnahorite, and with magnesium carbonate content up to around 30−35% (Table 2). The absence of superstructure 101, 015, and 021 reflections in XRD of the Ca−Mg kutnahorite-type carbonates indicated minor or no cation ordering.[20]

The spherulites obtained in solid media are quite different both texturally and compositionally from those obtained in liquid media from *Ch. marismortui* cultures,[16] which are made of aragonite and were also studied here for comparison. In liquid media, the aragonite spherulites formed together with struvite crystals. Aragonite spherulites are preferentially formed in liquid media by many different types of halophilic bacteria, and, in the studied case, they formed mainly within Biofilm supernatants in the upper part of the precipitation flasks whereas struvite crystal growth was found preferentially in the bottom of the flasks.[2]

As mineral kutnahorite is a Mn-rich Ca−Mg−(Fe) carbonate, the experiment with *Ch. marismortui* was repeated after adding to the culture a diluted solution of $MnCl_2 \cdot 4H_2O$. The resulting spherulites were similar, both texturally and compositionally, to those previously obtained from *Ch. marismortui* cultures without Mn salts.[16] In this case they were also made of calcian−magnesian carbonate with kutnahorite structure, but containing small amounts of Mn (Table 2) in the spherulite cores. According to EDX microanalysis, Mn substitutes Mg in the calcian−magnesian kutnahorite preferentially during the

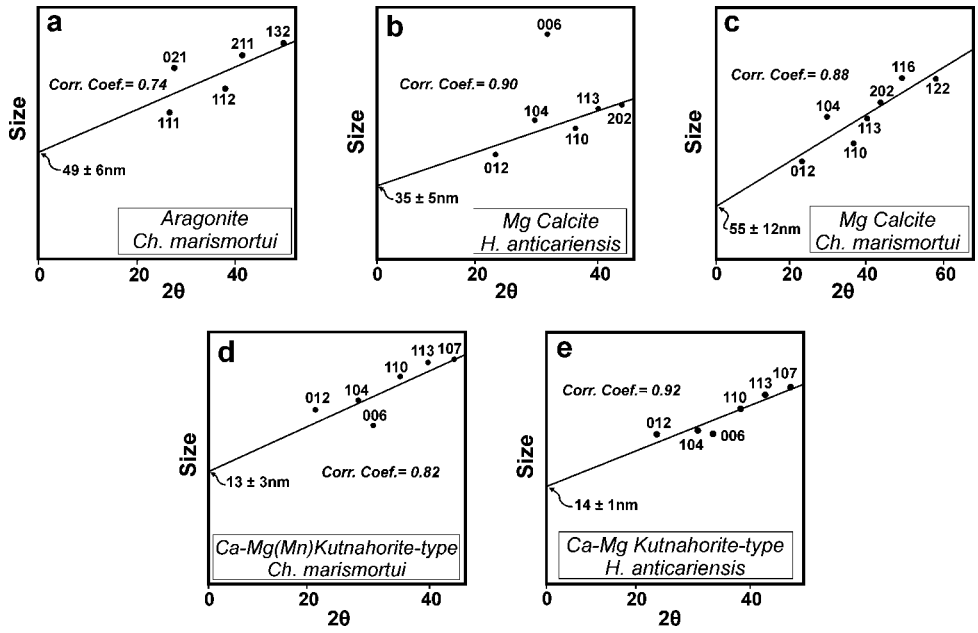

Figure 1. Coherent domain size versus 2θ angle for well-resolved XRD peaks of the samples studied. Correlation coefficient for the regression analysis is also indicated. Domain size is determined from the peak broadening (integral breadth).

earliest stages of spherulite accretion. Mn is incorporated always in very small amounts ($\leq$0.02 atoms of Mn per formula unit), at 7.5% and higher salt concentrations (Table 2). The $MgCO_3$ molar content of Ca−Mg kutnahorite-type carbonate ranged from 23 to 35%, whereas that of Ca−Mg−(Mn) kutnahorite-type carbonate was from 23 to 33%, with up to 2% of Mn in spherulite cores (Table 2).

The precipitates obtained from cultures of *H. anticariensis* at 7.5% salt concentration were texturally and compositionally quite similar to those precipitated by *Ch. marismortui* at the same and higher salt concentrations, either with or without Mn present in the medium. Nevertheless, the spherulites produced by *H. anticariensis* at 2.5% salt concentration were quite different, both texturally and compositionally, and consisted of magnesian calcite with low magnesian content (Table 2). Magnesian calcite spherulites from *Ch. marismortui* cultures at the same (2.5%) salt concentration had, however, higher Mg content (Table 2).

XRD Crystallinity Study. The textural and structural features (coherent domain size and refined unit-cell parameters) of the studied carbonate phases are summarized in Table 2. Crystallinity of spherulites made up of aragonite (Figure 1a) and magnesian calcite (Figures 1b and 1c) was much better than that of kutnahorite-type carbonates (Figures 1d,e). Coherent domain size of aragonite and magnesian calcites ranged from 30 to 67 nm, whereas that of the kutnahorite-type carbonates ranged from 10 to 15 nm (Table 2).

The peak broadening measure for 006 reflection in the magnesian calcite precipitated by *H. anticariensis* clearly deviates from the trend defined by the other reflections, and reveals that its crystallinity along the *c* crystallographic axis is lower than along any other direction (Figure 1b). Crystallinity measured for the magnesian calcite precipitated by *Ch. marismortui* was slightly higher.

The crystallinity along [001] of kutnahorite-type carbonates (either with or without Mn traces) was, however, comparable to that found for the other crystallographic directions (Figures 1d,e). A remarkable feature of the kutnahorite-type carbonates studied was the small size of their coherent domains, with values between 10 and 15 nm (Figures 1d,e; Table 2). The unit-cell dimensions of the two kutnahorite-type carbonates studied were much smaller than those of calcites (Table 2).

Texture and Crystal Growth Features. High-magnification secondary electron images of the surface of the aragonite spherulites precipitated in liquid media (Figure 2a) evidenced columnar-to-acicular crystal habits forming radial aggregates (Figures 2b,c). The columns grew at their tips (Figure 2e) by aggregation of rounded nanoparticles with sizes smaller than 100 nm (Figure 2e). These nanocrystal aggregates evolved downward to hexagonal plates, with larger sizes toward the interior of the spherulite (Figure 2f). Crystal coarsening resulted from the piling up of single hexagonal plates, corresponding to (001) pinacoidal faces, along the *c* crystallographic axis (Figures 2d,f).

The surface of magnesian calcite spherulites precipitated by *H. anticariensis*, either with or without organic pellicles (Figures 3a,b), was covered by rounded nanoparticles measuring usually less than 100 nm (Figures 3d−f), this resulting in rough surfaces (Figure 3c). Empty bacterial molds encapsulated by these nanocrystals were frequently preserved on spherulite surfaces (Figure 3d). When attached to gels, the nanoparticles did not show any organization (Figure 3e). Downward into the spherulite, just below the gel-rich zones (black arrow in Figure 3b), the nanoparticles showed a progressively better arrangement that tended to produce a radial pattern (Figure 3f). The radial structure was more clearly observed in spherulite surfaces without gels (Figure 4a) or in sections (Figure 4d). These surfaces were rough (Figure 4b), and the tips of the crystals defining the radial pattern showed a trigonal habit at their growth front (Figure 4c). In sections, the fibrous internal structure of the spherulites was more visible (Figure 4d). It was produced by the radial piling up of rounded growth units following the elongation of the aciculae (Figure 4e). These nanoparticles formed aciculae with triangular tips along the *c* axis (Figures 4c,f).

Similar textural features were visible in magnesian calcite spherulites precipitated by *Ch. marismortui* (Figure 5a). Some spherulites showed a very rough surface texture (Figure 5b) and

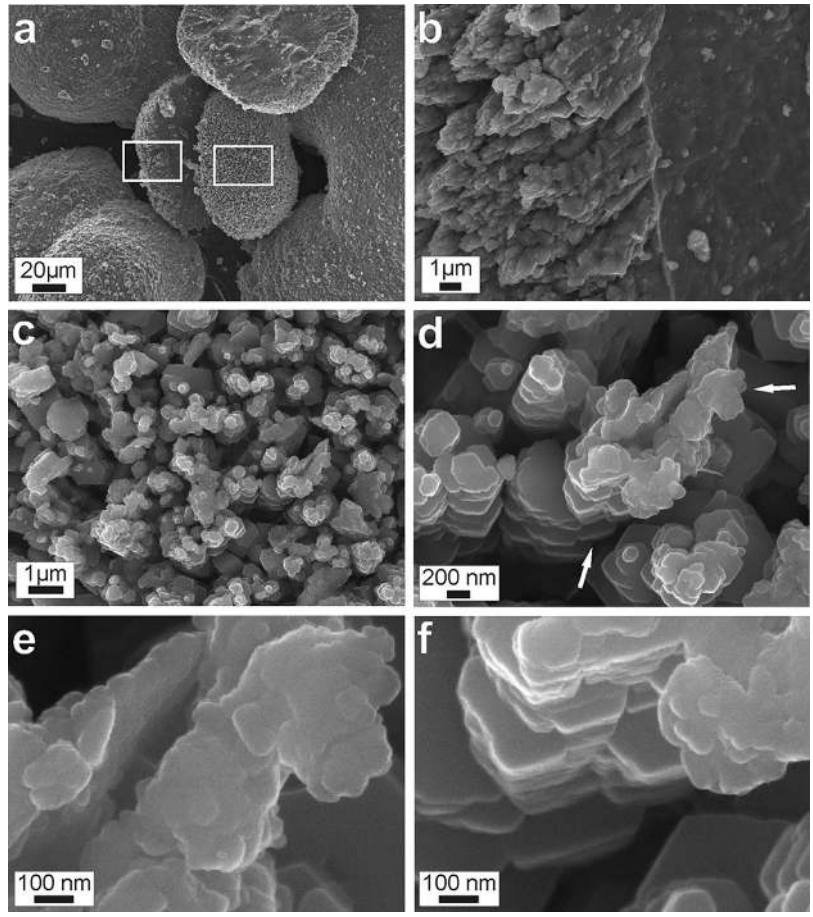

Figure 2. (a) Aragonite spherulites with spiny surfaces. Squares indicate the location of insets shown in (b) (left) and (c). (b) Oblique view of a spherulite surface made of radial aggregates of crystals. (c) Surface view of a spherulite showing the columnar habit and downward coarsening of aragonite crystals. (d) Higher magnification image of the lower-right part of (c). The upper part of the columns is formed by rounded growth units with a downward transition to larger crystals. Arrows points to the position of insets shown in (e) and (f). (e) Tip of a column in the upper right part of (d), formed by aggregation of rounded growth units less than 100 nm in size. (f) Transition from rounded nanocrystals (upper right corner) to hexagonal plates with size increasing downward. Plate surfaces are (001) pinacoidal faces piled up along their *c* crystallographic axis.

were formed by aggregates of mineralized bacterial molds with a preferred orientation perpendicular to the biolith surface (Figure 5c). Nanoparticles were also attached to gels (Figure 5c) and to former bacterial surfaces, displaying a radial growth pattern (Figures 5d−f).

Regardless of the bacterial culture where they precipitated, and of the presence or absence of Mn (Figures 6a,d), the surface of the Ca−Mg kutnahorite-type carbonate spherulites washed of organic gels revealed a completely different surface texture, consisting of a radial arrangement of tripod-like skeletal crystals (Figures 6b,e). These crystals were also composed of nanometer-sized rounded particles, but with slightly smaller diameter than that of nanoparticles observed in aragonite and magnesian calcite spherulites (Figures 6c,f). The arrangement of these nanoparticles leads to the formation of peculiar skeletal nanocrystal triaxial aggregates with the development of edges and vertices instead of faces in the crystal (Figures 6c,f).

Discussion

Influence of the Medium. The crystal-growth features described above for bacterial carbonate precipitates are similar to those of inorganic (abiotic) carbonates precipitated under controlled conditions by the counter diffusion of Ca^{2+} and CO_3^{2-} ions through a porous transport medium of silica gel with two solution reservoirs of $CaCl_2$ and Na_2CO_3.[5] In abiotic experiments without Mg, calcite forms first, and aragonite later. Rhombohedral crystals of calcite occur closest to the $CaCl_2$-bearing column (Ca-richer, and less saturated in CO_3^{2-}), and calcite spherulites forms toward the Na_2CO_3 reservoir. Aragonite is formed much later, only in the area closest to the Na_2CO_3 reservoir, and it exclusively develops spherulitic morphology. When the gels are doped with Mg^{2+}, $CaCO_3$ nucleation is inhibited, waiting (induction) time increases (mainly at low concentration), and magnesian calcite (instead of aragonite) spherulites form toward the Na_2CO_3 reservoir.[5]

In the experiments with bacteria, the system is formed by the agar-bearing Ca−Mg salts (in solid culture media) or by the solution (in liquid culture media), on the one hand, and by the bacterial aggregates and biofilms, on the other. The latter constitutes a CO_2 pumping system. Actually, the high CO_3^{2-} concentration necessary for carbonate precipitation in bacterially mediated $CaCO_3$ precipitates was driven by CO_2 emission controlled by bacterial metabolism, as no precipitates were observed in the control with noninoculated culture media. Irrespective of the nature of the medium and of their mineralogy, all the bacterial carbonate bioliths obtained developed spherulitic morphology, and carbonate precipitation invariably occurred close to bacterial surfaces.

In bacterial cultures made in liquid media, precipitation of aragonite spherulites is restricted to the more viscous bacterial

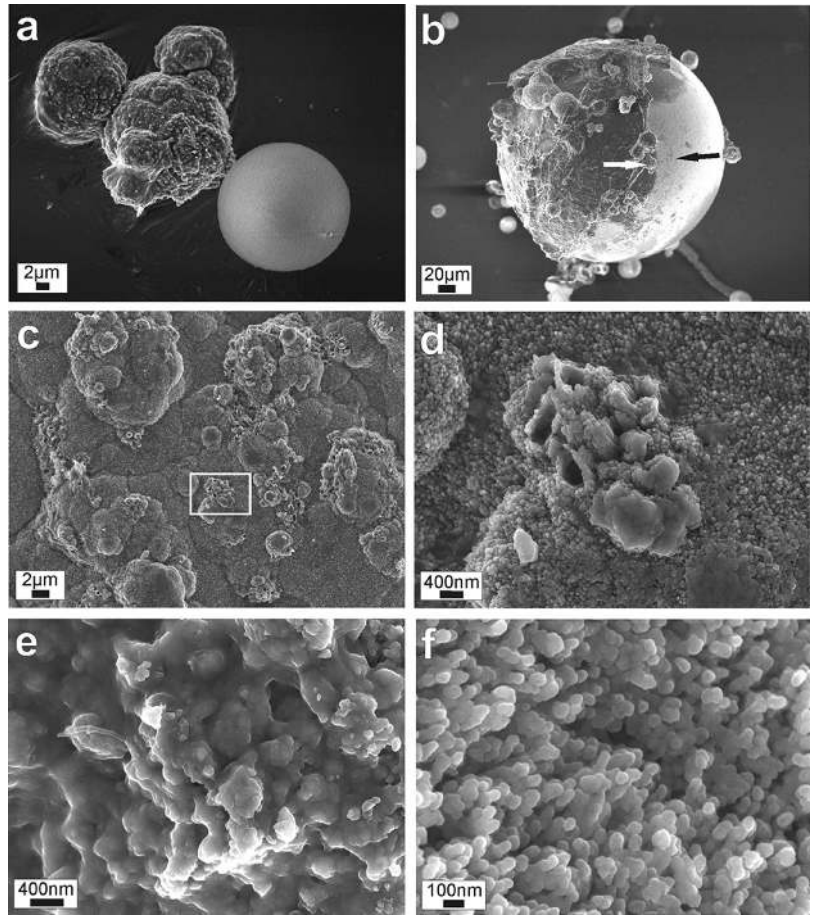

Figure 3. (a) Isolated (right) and grouped (by adhesion due to organic gels) magnesian calcite spherulites precipitated by *H. anticariensis*. (b) Spherulite partially uncovered by organic gels, and partially lumped by gels together with smaller spherulites. White and black arrows indicate the locations of the insets represented in (e) and (f), respectively. (c) Mammilated surface made of spherulites joined by gels full of nanocrystalline particles and bacterial molds. (d) Inset of the boxed area in (c), showing mineralized bacterial molds. (e) Thick organic gel coatings are full of nanocrystals of a few dozen nanometers in size. (f) The same units in the area without gels indicated by arrows in (b).

Biofilm, with the bulk solution acting as Ca^{2+} and Mg^{2+} reservoir, and the Biofilm acting as a source of CO_2. Nevertheless, Mg is not incorporated to the carbonate structure formed in these liquid media at any salinity. In cultures made in liquid media, Mg is precipitated exclusively as idiomorphic struvite crystals, mainly within the bulk solution, although it can locally form within the Biofilm.[16] Therefore, bacterial metabolism favors aragonite precipitation within the Biofim whereas struvite precipitation is here inhibited and mainly occurs in the remaining solution with higher Mg^{2+}/Ca^{2+}, where PO_4^{3-} and NH^{4+} ions produced during metabolization of organic nutrients are preferentially released.[21]

Precipitation of metastable Ca and Ca−Mg carbonate phases (aragonite, calcite rich in magnesium, dolomite, etc.) instead of pure calcite in natural environments and in biotic and abiotic experiments is classically explained by Mg inhibition of calcite precipitation.[11] Nevertheless, Rivadeneyra et al. have demonstrated that the inhibitory effect of Mg is less important in bacterial precipitation than in pure inorganic precipitation.[22] Moreover, this effect is much lower in moderately halophilic bacteria than in nonhalophilic ones.[23] Organic compounds forming bacterial walls and biofilms absorb Ca with greater intensity than Mg, thus reducing Ca activity within, and around, organic pellicles.[24] This creates strong Ca concentration gradients from bulk solution toward bacterial surface microenvironments. In solid media, the increase in Mg content observed from magnesian calcite to Ca−Mg(−Mn) kutnahorite-type carbonate spherulites precipitated in progressively more saline solid media correlates to the increase in spherulite surface roughness (compare Figures 4c,f with Figures 6c,f), and to the parallel decrease in crystalline mosaic size (Table 2). The lower crystallinity of the carbonate phases increasingly richer in Mg (and eventually with Mn), precipitated in more viscous solid media, suggests a faster growth rate than that of the aragonite with higher crystallinity, precipitated within the less viscous Biofilm microenvironment formed in liquid media.

In summary, both in inorganic and in biomediated carbonate precipitation systems the existence of highly viscous media fosters the development of spherulitic instead of polyhedral morphologies, the incorporation of Mg (and of Mn) to $CaCO_3$ crystals, and the formation of anhydrous trigonal Ca−Mg carbonates with calcite structure instead of aragonite. High supersaturation gradients, resulting from the slow transport properties of viscous media with low porosity, lead to local high supersaturation and growth rates of the precipitated mineral phases.[25] We interpret that, in solid media, precipitation of magnesian calcite (and of Ca−Mg−Mn kutnahorite-type carbonates at higher salinity) instead of aragonite is encouraged by the higher Ca (Mg) supersaturation gradient promoted by the limited mobility of solutes in such transport media.

Crystal Growth in Bacterial Precipitation of Carbonates. Spherulitic and dendritic morphologies are typical features of crystals formed at extremely high growth rates, and result from highly nonequilibrium processes operating in the culture

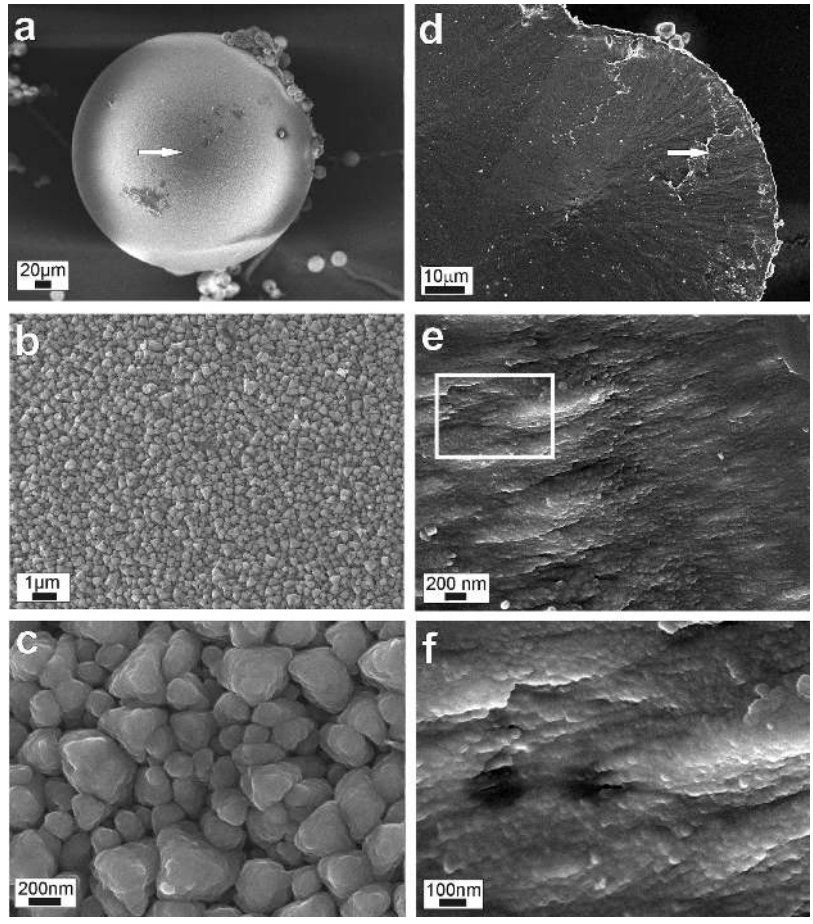

Figure 4. (a) Magnesian calcite spherulite precipitated by *H. anticariensis* without gels (present only in darker patches). (b) High magnification image of the point indicated by an arrow in (a), showing the texture of the surface of the spherulite, which is a uniaxial aggregate of crystals. (c) Close-up of (b), showing the triangular tips of the crystals, with rough surfaces resulting from the adhesion of rounded nanocrystals. (d) View of the base of a spherulite detached from the glass surface of the precipitation flask, showing a radial growth pattern. (e) This inset of the point indicated by an arrow in (c) shows that the radial pattern is defined by the adhesion of rounded nanocrystals similar in size to those observed in (c). (f) Rounded nanocrystals in the area boxed in (e).

media, whereas polyhedral morphologies of $CaCO_3$ crystals form closer to equilibrium conditions.[26] Biolith accretion starts at the interface between medium and bacterial aggregates, regardless of the mineralogy of the precipitates and of the viscosity of the culture medium. There, the highest CO_2 concentration is reached, promoting nucleation of nanocrystalline units. Later on, spherulitic morphologies develop by adhesion of these nanoparticles.

Crystal growth proceeds not only by deposition of ions and molecules but also by adhesion of small crystal seeds.[27,28] In this type of growth, nanocrystals rotate and orient in appropriate ways before final attachment to the growing surface.[29] Oriented attachment of nanocrystals is usually described in precipitation media bearing organic additives, although they are not essential for this kind of growth mechanism.[30] Important vectorial long-ranged (van der Waals or dipolar) interactions take place between the nanoparticles, which finally form mesocrystals.[8] The nanocrystals observed in all studied carbonate precipitates, whether aragonite (Figure 2f), magnesian calcite (Figures 3e,f, 4c,f, 5c,f) or Ca−Mg kutnahorite-type carbonates with or without Mn traces (Figures 6c,f), constitute crystal seeds of mesocrystals. These nanoparticles have very small sizes (tens to a few hundred nm) and rounded morphology, which tends to minimize their surface energy.

The occurrence of nanocrystal building units is clearly related to the presence of bacterial aggregates (Figures 3d, 5d) and organic gels (Figures 3b,e,f, 4c) on spherulite surfaces. Crystallization of the studied bacterial spherulitic mesocrystals occurs when nanoparticles are stabilizated by organic colloids. In gels, mesocrystals form under very high supersaturation, which promotes the nucleation of very small building units, and the lack of turbulence in these media also favors interactions between nanoparticles.[8] Higher supersaturation explains the smallest size of nacrystal building units and of crystalline mosaic size in the studied bacterial precipitates formed in solid culture media (Table 2, Figures 1, 6). Tripod-like morphologies in the surface of the studied Ca−Mg kutnahorite-type carbonate spherulites (Figure 6) result from the structural control on the polarization of nanocrystals along different crystallographic directions.

In magnesian calcite and aragonite spherulites, the radial texture of nanocrystal aggregates is due to a geometrical selection process, which favors specific crystallographic orientations in relation to the substrate (Figures 2d−f, 4d−f and 5d−f). This texture develops when the fastest crystal-growth direction (*c* crystallographic axis) is perpendicular to the surface of the spherulite. Fast growth along the *c* axis in magnesian calcite spherulites precipitated by *H. anticariensis* is also evidenced by the data obtained from the XRD peak-profile analysis (Figure 1b). High growth rates normal to (001) crystallographic planes explain the smaller value of the size of coherent domain for the (006) peak in relation to regression value found for the other reflections. Nevertheless, a preferential crystal growth along the

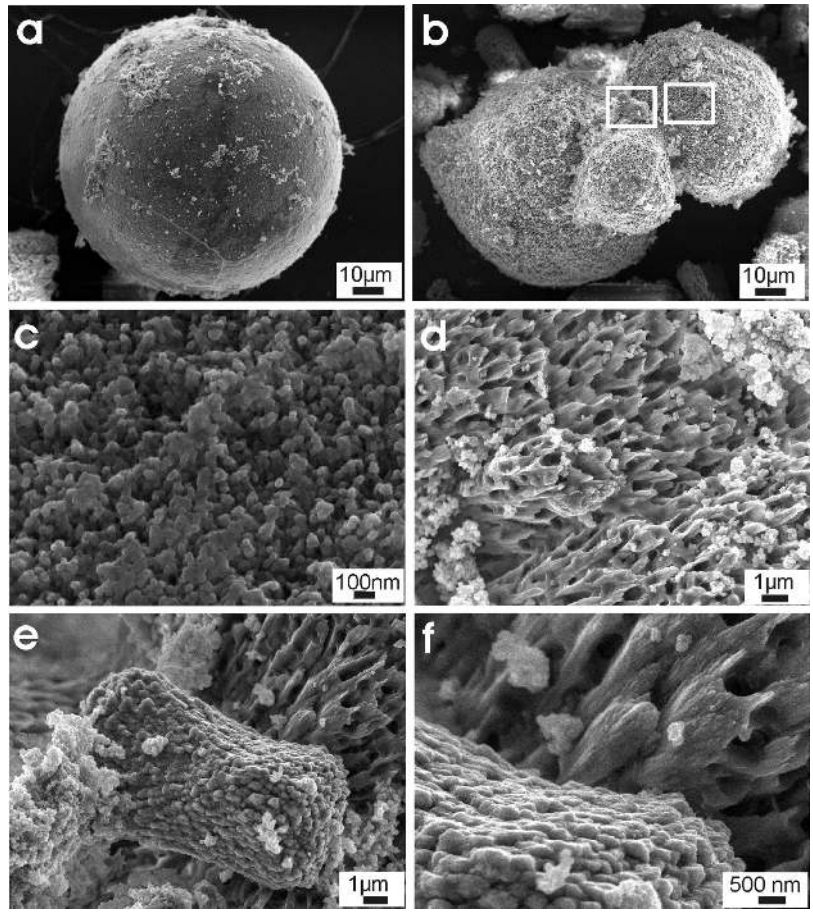

Figure 5. Magnesian calcite spherulites precipitated by *Ch. marismortui*. (a) Isolated spherulite partially surrounded by gels. (b) Biolith with a rough surface with less abundant gels. The boxed areas correspond to insets shown in (d) (right) and (e). (c) Nanoparticles attached to gels in the surface of (a). (d) This enlarged oblique view shows an aggregate of mineralized bacterial molds with a preferential orientation perpendicular to the biolith surface (compare with Figure 3d). (e) Dumbbell-shaped object formed by an aggregate of nanocrystals with similar texture to those of Figure 4b. (f) Detail of (e); showing mineralized bacterial mold within a radial pattern growth defined by nanometric particles similar to those visible in Figure 4e.

c axis is less evident in magnesian calcite with higher crystallinity and Mg content, precipitated by *Ch. marismortui*, and in the other Ca−Mg kutnahorite-type carbonates (with or without Mn) precipitated either by *Ch. marismortui* or by *H. anticariensis*. The fastest crystal growth occurs in Ca−Mg(Mn) kutnahorite-type carbonates, as confirmed by their lowermost coherent domain size (Table 2). Fast crystal growth of Ca−Mg(Mn) kutnahorite-type carbonates occurred not only along the *c* axis but also along the other crystallographic directions, as demonstrated by the good correlation of the (006) peak width with the other directions (Figures 1d,e).

Relation between Composition, Texture and Structure. The role of magnesium in calcium carbonate precipitation has been the object of many studies.[31] In general, magnesian calcite crystals, both natural and experimentally precipitated, show rough interfaces and, when faces are present, they are poorly developed.[32] In porous abiotic media, the increase in Mg^{2+} as well as in other more electronegative divalent cations, like Mn^{2+}, prompts the development of this type of morphology in the calcite precipitates.[6]

Magnesium content increases from magnesian calcite to Ca−Mg(Mn) kutnahorite-type carbonate, and/or to "protodolomite" as the Mg-richest end-member.[16] The latter should be rather named "highly disordered dolomite" because the term "proto-dolomite" should be avoided.[33] Poor cation ordering and Ca enrichment are characteristic crystal chemical features of abiogenic Ca−Mg carbonate precipitates at low temperatures.[20] Biogenic materials have even greater Ca−Mg disorder, as observed in the bacterial Ca−Mg carbonates studied, and can be sometimes formed by amorphous calcium carbonate precursors.[9]

At crystal surfaces, crystal growth from solution involves replacement of solvent molecules by solute particles, while crystal dissolution involves exactly the opposite. Solvent (water) attack consists basically of an acid attack by the hydrogen of the water molecules on the oxygen atoms of the polyatomic anions (CO_3^{2-}).[34] Hydrogen-bridged bonds with oxygen atoms are easier to be formed in magnesian-rich calcite relative to pure calcite. The O−H bond is weaker in progressively stronger oxyacids. In salts of strong acids, the bond between oxygen and metal is also weak; and the weaker the metal−oxygen bond, the stronger is the bond between oxygen and nonmetal or metalloid elements (the most electronegative cations in the salts).[35] Therefore, the strength of the carbonic acid related to carbonate precipitation is greater in calcite than in magnesite (or in aragonite, see below). The strength of carbonic acid is monitored by the strength of the C−O bond in the CO_3 group.

The entrance of magnesium in the calcite structure implies a contraction of the unit cell.[36] This is evidenced by the a = 4.875−4.879 Å and c = 16.334−16.375 Å values obtained for Ca−Mg kutnahorite-type carbonates (Table 2), which are intermediate between those of magnesite (a = 4.632 Å and c

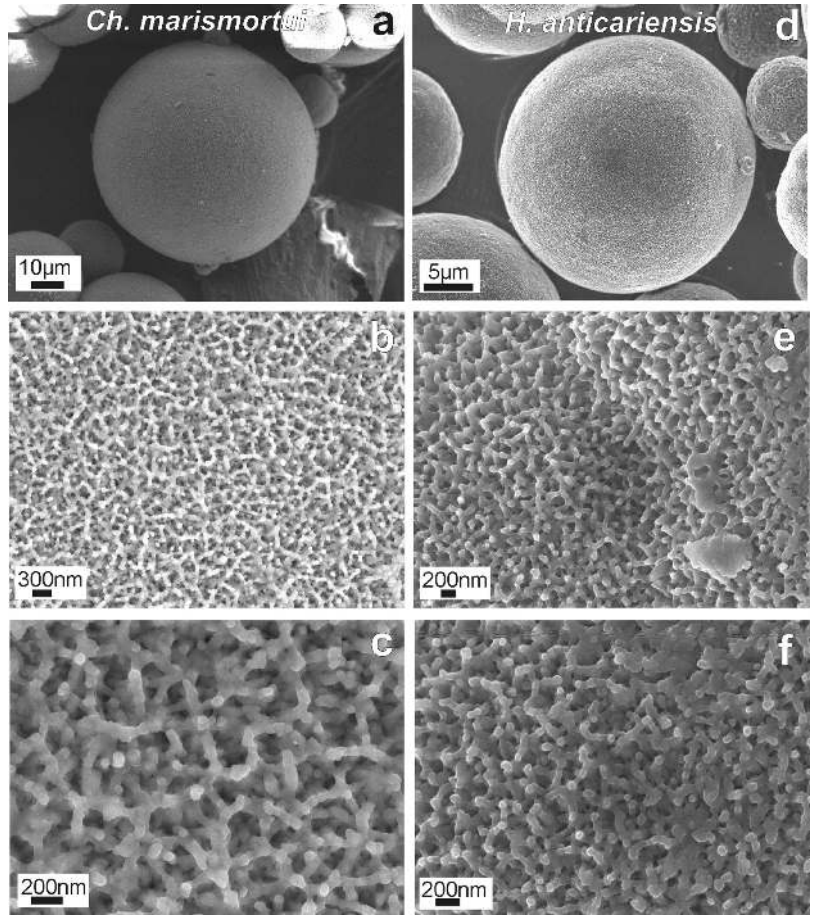

Figure 6. Secondary electron images of Ca−Mg kutnahorite-type carbonates with and without Mn traces, respectively, precipitated by *Ch. marismortui* (a,b,c) and *H. anticariensis* (d,e,f). Low magnification images (a,d) reveal the same shape and size of the spherulites. At higher magnification (b,d) both types of spherulites show the same kind of rough and porous surface. At the highest resolution (c,f) the same type of tripod-like branched microstructure is formed by the adhesion of rounded nanoparticles in both cases.

Table 3. Interatomic Distances (Å) and Angles (deg) in the Anion Sublattice of Calcite, Magnesite, and Aragonite Structures, Determined from Structural Refinement Data with the ORTEP III Program[38]

	distances and angles in the CO_3 groups		nonbonded distances	
mineral	C−O	O−C−O	C−C	O−O
calcite	1.282	120	4.05	3.26
magnesite	1.285	120	3.66	2.92
aragonite	1.278 (×1)−1.284 (×2)	119.5−120.2	2.88	2.74−3.06

= 15.002 Å) and of calcite (a = 4.988 Å and c = 17.068 Å).[37,38] When magnesite and calcite structures are compared, the lattice contraction due to the crystal chemical substitution of Mg for Ca leads to a reduction in the divalent cation−oxygen distances across the cation and anion layers, which are perpendicular to the c crystallographical axis. It also results in a reduction of the distances between CO_3 groups ("nonbonded" distances) within individual anionic layers (Table 3). Reduction of the "nonbonded" distances is countered by an increase of the C−O distance within CO_3 groups (Table 3). This structural contraction is illustrated in Figure 7, both across and along the c axis.

In carbonate minerals, the oxygens of the CO_3 groups are surrounded by two or by three cations. In the calcite structure, oxygen is coordinated by two Ca. In the aragonite structure, oxygen is coordinated by three Ca. In the magnesite structure, oxygen is coordinated by two Mg, which is more electronegative than Ca. According to orbital interpretation of the Zachariasen−Baur extension of the Pauling's second rule, oxygen atoms in aragonite and magnesite structures are *overbonded* because they prefer to have a smaller coordination number or to be coordinated by more electropositive cations in more stable structures (such as calcite).[39] *Overbonded* oxygens seem compact better due to the reduction of "nonbonded repulsion" (equivalent to "Pauli repulsion") between oxygens, as indicated by the reduction of the distance between CO_3 groups in aragonite and magnesite (Table 3). Therefore, the density of the carbonate increases due to the contraction of the anionic (CO_3^{2-}) sublattice from calcite to aragonite and to magnesite.

At ambient pressure the increase in the number of electrons of the system produce an insulator-to-metal transition (that is, metallization) among other possible effects. Electron count-driven metallization in solutions has been illustrated by many studies.[40] In the studied bacterial carbonate precipitates, the high salinity (alkalinity) of the solution changes drastically the electronic environment of the CO_3 groups. Dissolution of alkali metals (M) and formation of ion pairs ($M^+ \cdot e^-$) of very short lifetime[41] provides a transient electron excess in the studied bacterial culture media, and adds electrons to the CO_3 system. The increase of the electron count produces the population of empty high energy C−O antibonding orbitals, which weakens C−O bonds, and seems to induce a reduction in the "nonbonded repulsions" between the CO_3 groups: the ratio of the nonbonded (O−O and C−C) to bonded (C−O) distances decreases from calcite structure to denser aragonite and magnesite structures (Table

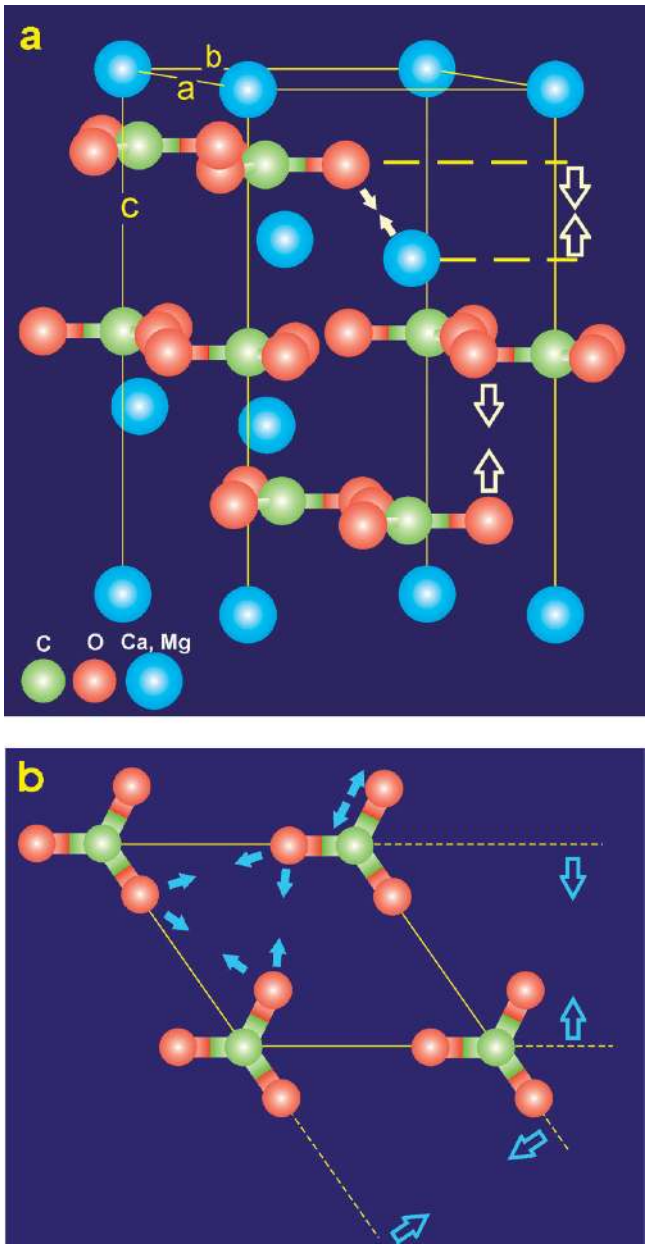

Figure 7. Ball-and-stick model drawing of the calcite structure parallel and perpendicular to the *c* axis. Structural contraction associated with the Ca substitution by Mg leads to decreased reticular distances (blank arrows) and nonbonded and bonded distances (solid arrows).

3). In elemental solids, the decrease of the ratio of the nonbonded to bonded distances leads to a structural compaction process that is called sometimes metallization.[42] Therefore, the increase of electron count must encourage the formation of denser carbonates, like aragonite in liquid media and Ca−Mg carbonates increasingly richer in Mg in solid media, instead of the thermodynamically stable mineral calcite. Electronic properties, such as the polarizability and the dipole moments of the nanoparticles, increase drastically in this type of solution: nonbonded (dipolar, van der Waals) interactions between adjacent nanobuilding-blocks are more effective and, consequently, the proposed aggregation-based crystallization mechanism is favored over other crystal-growth mechanisms, such as surface nucleation growth and spiral growth, for which bonded interactions constitute the main chemical forces.

Acknowledgment. We thank Alicia González and Isabel Guerra from the Scientific Instrumentation Center of the University of Granada and to Angel Caballero for his technical drawing. This work was financed by the Research Projects CGL2005-03887 and CGL2007-66744-CO2-O1 (S.E.U.I.D.-M.C.T., Spain) and is a contribution of the Research Groups RNM 208 and 179 of the Junta de Andalucía and of CO2SolStock (European Commission). The authors gratefully acknowledge the critical reviews and useful comments of two anonymous reviewers.

References

(1) (a) Ehrlich, H. L. *Geomicrobiology*; 4th ed.; Marcel Dekker: New York, 2002. (b) Lowenstam, H. A.; Weiner, S. *On Biomineralization*; Oxford University Press: Oxford, 1989.
(2) Rivadeneyra, M. A.; Delgado, R.; Parraga, J.; Ramos-Cormenzana, A.; Delgado, G. *Folia Microbiol.* **2006**, *51*, 445–453.
(3) (a) Sánchez-Román, M.; Rivadeneyra, M. A.; Vasconcelos, C.; McKenzie, J. A. *FEMS Microbiol. Ecol.* **2007**, *61*, 273–284. (b) Sánchez-Román, M.; Vasconcelos, C.; Schmid, T.; Dittrich, M.; McKenzie, J. A.; Zenobi, R.; Rivadeneyra, M. A. *Geology* **2008**, *36*, 879–882. (c) Chen, L.; Shen, Y.; Xie, A.; Huang, B; Jia, R.; Guo, R.; Tang, W. *Cryst. Growth Des.* **2009**, *9*, 743–754.
(4) (a) Riding, R. E. *Sedimentology* **2000**, *47*, 179–214. (b) Reid, R. P.; Visscher, P. T.; Decho, A. W.; Stolz, J. F.; Bebout, B. M.; Dupraz, C.; Macintyre, I. G.; Paerl, H. W.; Pickney, J. L.; Prufert-Bebout, L.; Steppe, T. F.; DesMarais, D. J. *Nature (London)* **2000**, *406*, 989–992.
(5) Fernández-Díaz, L.; Putnis, A.; Prieto, M.; Putnis, C. *J. Sediment. Res.* **1996**, *66*, 482–491.
(6) Fernandez-Diaz, L.; Astilleros, J. M.; Pina, C. M. *Chem. Geol.* **2006**, *225*, 314–321.
(7) Sindhu, S.; Jegadesan, S.; Edward-Leong, R. A.; Valiyaveettil, S. *Cryst. Growth Des.* **2006**, *6*, 1537–1541.
(8) Cölfen, H.; Antonietti, M. *Angew. Chem., Int. Ed.* **2005**, *44*, 5576–5591.
(9) (a) Raz, S; Addadi, L.; Weiner, S. *Adv. Mater.* **2000**, *12*, 38–42. (b) Addadi, L.; Raz, S.; Weiner, S. *Adv. Mater.* **2003**, *15*, 959–970. (c) Weiner, S.; Levi-Kalisman, Y.; Raz, S.; Addadi, L. *Connect. Tissue Res.* **2003**, *44*, 214–218. (d) Raz, S.; Hamilton, P. C.; Wilt, F. H.; Weiner, S.; Addadi, L. *Adv. Funct. Mater.* **2003**, *13*, 480–486. (e) Ajikumar, P. K.; Wong, L. G.; Subramanyam, G.; Lakshminarayanan, R.; Valiyaveettil, S. *Cryst. Growth Des.* **2005**, *5*, 1129–1134. (f) Sondi, I.; Škapin, S. D.; Salopek-Sondi, B. *Cryst. Growth Des.* **2008**, *8*, 435–441.
(10) Aloisi, G.; Gloter, A.; Krüger, M.; Wallmann, K.; Guyot, F.; Zuddas, P. *Geology* **2006**, *34*, 1017–1020.
(11) (a) Berner, R. A. *Principles of Chemical Sedimentology*; McGraw-Hill: New York, 1971. (b) Putnis, A. *Introduction to Mineral Sciences*; Cambridge Univ. Press: Cambridge, 1992. (c) Morse, J. W.; Mackenzie, F. T. *Geochemistry of Sedimentary Carbonates*; Elsevier: Amsterdam, 1990. (d) Morse, J. W. In *Sediments, Diagenesis and Sedimentary Rocks*; Mackenzie, F. T., Ed.; Elsevier: Amsterdam, 2005; Vol. 7, pp 67−85.
(12) (a) Paquette, J.; Reeder, R. J. *Geochim. Cosmochim. Acta* **1995**, *59*, 735–749. (b) Astilleros, J. M.; Pina, C. M.; Fernández-Díaz, L.; Putnis, A. *Geochim. Cosmochim. Acta* **2002**, *66*, 3177–3189. (c) Hu, X. M.; Grossie, D. A.; Higgins, S. R. *Am. Mineral.* **2005**, *90*, 963–968.
(13) Folk, R. L. *J. Sediment. Petrol.* **1974**, *44*, 40–53.
(14) Given, R. K.; Wilkinson, B. H. *J. Sediment. Petrol.* **1985**, *55*, 109–119.
(15) Chernov, A. A. *Crystal Growth. Modern Crystallography III*; Springer-Verlag: Berlin,1984.
(16) Rivadeneyra, M. A.; Martín-Algarra, A.; Sánchez-Navas, A.; Martín-Ramos, J. D. *Geomicrobiol. J.* **2006**, *23*, 1–13.
(17) (a) Ventosa, A.; Gutierrez, M. C.; García, M. T.; Ruiz-Berraquero, F. *Int. J. Syst. Bacteriol.* **1989**, *39*, 382–385. (b) Martínez-Cánovas, M. J; Béjar, V.; Martínez-Checa, F.; Quesada, E. *Int. J. Syst. Evol. Microbiol.* **2004**, *54*, 1329–1332.
(18) Martín, J. D. *Using XPowder—a sofware package for powder X-ray diffraction analysis*; D.L. GR-1001/04; ISBN: 84-609-1497-6; Spain, 2004. (Also available at http://www.xpowder.com.).
(19) Klug, H. P.; Alexander, L. E. *X-ray Diffraction Procedures for Polycrystalline and Amorphous Materials*; John Wiley: New York, 1973..
(20) Ardvison, R. S.; MacKenzie, F. T. *Am. J. Sci.* **1999**, *299*, 257–288.

(21) (a) Rivadeneyra, M. A.; Pérez-García, I.; Ramos-Cormenzana, A. *Curr. Microbiol.* **1992**, *24*, 343–347. (b) Rivadeneyra, M. A.; Pérez-García, I.; Ramos-Cormenzana, A. *Geomicrobiol. J.* **1992**, *10*, 125–137.
(22) Rivadeneyra, M. A.; Ramos-Cormenzana, A.; García-Cervigón, A. *Can. J. Microbiol.* **1985**, *31*, 229–231.
(23) Ferrer, M. R.; Quevedo-Sarmiento, J.; Béjar, V.; Delgado, R.; Ramos-Cormenzana, A.; Rivadeneyra, M. A. *Geomicrobiol. J.* **1988**, *6*, 49–57.
(24) (a) Wolt, J. D. *Soil Solution Chemistry: Applications to Environmental Science and Agriculture*; Wiley: New York, 1994. (b) Maier, R. M.; Pepper, I. L.; Gerba, Ch. P. *Environmental Microbiology*; Academic Press: San Diego, 2000.
(25) Putnis, A.; Prieto, M.; Fernández-Díaz, L. *Geol. Mag.* **1995**, *132*, 1–13.
(26) Gránásy, L.; Pusztai, T.; Tegze, G.; Warren, J. A.; Douglas, J. F *Phys. Rev.* **2005**, *E 72*, 011605–2005.
(27) Kostov, I.; Kostov, R. I. *Crystal habits of minerals*; Pensoft: Sofia, 1999.
(28) Shen, Q.; Wei, H.; Wang, L.; Zhou, Y.; Zhao, Y.; Zhang, Z.; Wang, D.; Xu, G.; Xu, D. *J. Phys. Chem. B* **2005**, *109*, 18342–18347.
(29) (a) Alivisatos, A. *Science* **2000**, *289*, 736–737. (b) Bandfield, J.; Welch, S.; Zhang, H.; Ebert, T. T.; Penn, R. L. *Science* **2000**, *289*, 751–754. (c) Grassmann, O.; Neder, R. B.; Putnis, A.; Löbmann, P. *Am. Mineral.* **2003**, *88*, 647–652.
(30) Zhang, Q.; Liu, S. J.; Yu, S. H. J. *Matter. Chem.* **2009**, *19*, 191–207.
(31) (a) Berner, R. A. *Geochim. Cosmochim. Acta* **1975**, *39*, 489–504. (b) Mucci, A. *Geochim. Cosmochim. Acta* **1986**, *50*, 2255–2265. (c) Fallini, G.; Gazzano, M.; Ripamonti, A. *J. Cryst. Growth* **1994**, *137*, 577–584.
(32) (a) Reddy, M.; Nancollas, G. H. *J. Cryst. Growth* **1976**, *35*, 33–38. (b) Gonzalez, L. A.; Carpenter, S. J; Lohmann, K. C. *J. Sediment. Petrol.* **1992**, *62*, 382–399.
(33) Kelleher, I. J.; Redfern, S. A. T. *Mol. Simul.* **2002**, *28*, 557–572.
(34) Gutmann, V. *The donor-acceptor approach to molecular interactions*; Plenum Press: New York, 1978.
(35) Ramberg, H. *J. Geol.* **1952**, *60*, 331–355.
(36) Althoff, P. L. *Am. Mineral.* **1977**, *62*, 772–783.
(37) (a) Maslen, E. N.; Streltsov, V. A.; Streltsova, N. R. *Acta Crystallogr. B* **1993**, *49*, 636–641. (b) Maslen, E. N.; Streltsov, V. A.; Streltsova, N. R.; Ishizawa, N. *Acta Crystallogr. B* **1995**, *51*, 929–939.
(38) Farrugia, L. J. *J. Appl. Crystallogr.* **1997**, *30*, 565.
(39) Burdett, J. K.; McLarnan, T. J. *Am. Mineral.* **1984**, *69*, 601–621.
(40) (a) Edwards, P. P.; Sienko, M. J. *Acc. Chem. Res.* **1982**, *15*, 85–93. (b) Edwards, P. P.; Sienko, M. J. *J. Chem. Educ.* **1983**, *60*, 691–696. (c) ThompsonJ. C. *Electrons in liquid ammonia*; Clarendon Press: New York, 1976.
(41) (a) Schindewolf, U. *Angew. Chem., Int. Ed. Engl.* **1968**, *7*, 190–203. (b) Dye, J. L. *Science* **2003**, *301*, 607–608.
(42) (a) Harrison, W. A. *Electronic Structure and the Properties of Solids*; Dover Publications: New York, 1989. (b) Burdett, J. K. *Chemical Bonding in Solids*; Oxford University Press: New York, 1995.

CG801320P